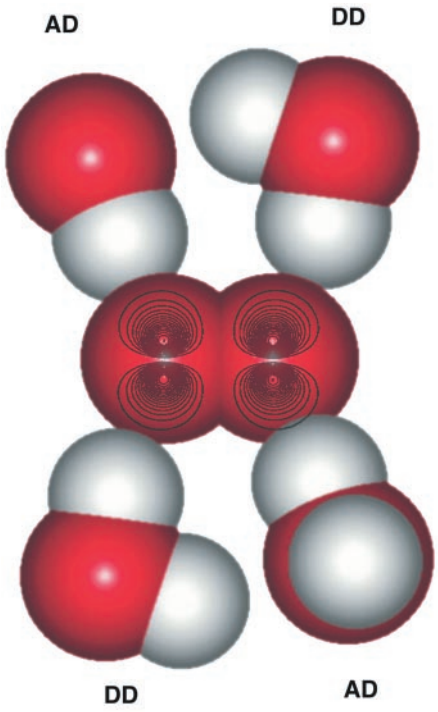

Fig. 3. Calculated minimum energy structure of $O_2^- \cdot (H_2O)_4$. The electron probability density of the π^* orbital is indicated by contours. DD is donor-donor roles and AD is acceptor-donor roles of the constituent water molecules.

interaction with four protons persists in the bulk, just as in our structure of the tetracoordinate hydration shell. Symons *et al.* (*8*) suggested that this saturation upon complexation with only four of the eight available lobes of the degenerate π^* orbital arises because the degeneracy is broken by solvation. This lowers the energy of the configuration where the electron pair occupies the π^* orbital oriented in the plane of the ionic H bonds. It is an open question how these water molecules interact with the higher solvation shells, and this topic is presently being addressed through the study of the larger clusters.

References and Notes

1. C. Schöneich, *Exp. Gerontol.* **34**, 19 (1999).
2. D. Salvemini *et al.*, *Science* **286**, 304 (1999).
3. R. G. Keese, N. Lee, A. W. Castleman Jr., *J. Geophys. Res.* **84**, 3791 (1979).
4. D. W. Fahey, H. Bohringer, F. C. Fehsenfeld, E. E. Ferguson, *J. Chem. Phys.* **76**, 1799 (1982).
5. X. Yang and A. W. Castleman Jr., *J. Am. Chem. Soc.* **113**, 6766 (1991).
6. P. Ayotte, G. H. Weddle, J. Kim, M. A. Johnson, *Chem. Phys.* **239**, 485 (1998).
7. P. Ayotte, S. B. Nielsen, G. H. Weddle, M. A. Johnson, *J. Phys. Chem. A* **103**, 10665 (1999).
8. M. C. R. Symons, G. W. Eastland, L. R. Denny, *J. Chem. Soc. Faraday I* **76**, 1868 (1980).
9. P. A. Narayana, D. Suryanarayana, L. Kevan, *J. Am. Chem. Soc.* **104**, 3552 (1982).
10. W. G. Mallard, Ed., *NIST Standard Reference Database Number 69, Feb. 2000 Release* (Gaithersburg, MD, 1998) (webbook.nist.gov/chemistry).
11. M. A. Johnson and W. C. Lineberger, in *Techniques for the Study of Gas-Phase Ion Molecule Reactions*, J. M. Farrar and W. Saunders, Eds. (Wiley, New York, 1988), pp. 591–635.
12. C. J. Gruenloh *et al.*, *Science* **276**, 1678 (1997).
13. K. T. Kuwata, Y. B. Cao, M. Okumura, *J. Phys. Chem. A* **102**, 503 (1998).
14. P. Ayotte, G. H. Weddle, M. A. Johnson, *J. Chem. Phys.* **110**, 7129 (1999).
15. S. S. Xantheas, *J. Phys. Chem.* **100**, 9703 (1996).
16. J. Sadlej, V. Buch, J. K. Kaziminski, U. Buck, *J. Phys. Chem. A* **103**, 4933 (1999).
17. P. Ayotte, G. H. Weddle, J. Kim, M. A. Johnson, *J. Am. Chem. Soc.* **120**, 12361 (1998).
18. P. Ayotte, J. A. Kelley, S. B. Nielsen, M. A. Johnson, *Chem. Phys Lett.* **316**, 453 (2000).
19. L. A. Curtiss, C. A. Melendres, A. E. Reed, F. Weinhold, *J. Comput. Chem.* **7**, 294 (1986).
20. P. Ayotte, thesis, Yale University, New Haven, CT (1999).
21. M. J. Frisch *et al.*, *Gaussian 94, Revision E.1* (Gaussian, Pittsburgh, PA, 1995).
22. We gratefully acknowledge support from the Experimental Physical Chemistry Division of the NSF. We thank W. H. Robertson for valuable technical assistance in the acquisition of data related to this work, and P.A. thanks Fonds pour la Formation de Chercheurs et de l'Aide à la Recherche Bourse Doctorale (FCAR-Québec).

7 December 1999; accepted 10 February 2000

Hot and Dry Deep Crustal Xenoliths from Tibet

Bradley R. Hacker,[1] Edwin Gnos,[2] Lothar Ratschbacher,[3] Marty Grove,[4] Michael McWilliams,[5] Stephen V. Sobolev[6] Jiang Wan,[7] Wu Zhenhan[7]

Anhydrous metasedimentary and mafic xenoliths entrained in 3-million-year-old shoshonitic lavas of the central Tibetan Plateau record a thermal gradient reaching about 800° to 1000°C at a depth of 30 to 50 kilometers; just before extraction, these same xenoliths were heated as much as 200°C. Although these rocks show that the central Tibetan crust is hot enough to cause even dehydration melting of mica, the absence of hydrous minerals, and the match of our calculated *P*-wave speeds and Poisson's ratios with seismological observations, argue against the presence of widespread crustal melting.

The processes that formed the Tibetan Plateau—the highest and largest topographic feature on Earth, and the archetypal signature of continent-continent collision—remain unclear. Models of wholesale underthrusting of India (*1*), lower crustal flow (*2*), intracontinental subduction (*3, 4*), or distributed shortening followed by convective thinning of thickened mantle lithosphere (*5*) make predictions about the thickening, heating, and melting histories of the plateau, but we have little direct knowledge of, for example, the thickness and thermal regime of Tibetan crust during much of the Cenozoic. The ages of crustal extension (*6*), crustal shortening (*7*), rapid upper crustal cooling (*8*), and potassic volcanism (*9*) have all been used to infer when the Tibetan Plateau attained its present thickness of 60 to 75 km, but few studies quantify crustal thickness or thermal gradient. Moreover, the presence of potassic volcanism has been causally linked to convective thinning of overthickened mantle lithosphere—and this seemed a plausible explanation when volcanism appeared to be only 13 million years (My) old and younger. However, recent reports (*10*) reveal that this style of volcanism has occurred in Tibet for 45 My, which calls into question the role of convective thinning, which should be an event with a time scale of about 5 My (*11*). Here we report a detailed analysis of xenoliths from the Tibetan Plateau, which reveal that the lower crust includes anhydrous metasedimentary granulite-facies rocks equilibrated at temperatures of 800° to 1100°C at depths of 30 to 50 km.

Alkalic volcanic rocks have erupted on the Tibetan Plateau since at least 45 million years ago (Ma) (Fig. 1). The most widespread and common are shoshonitic to ultrapotassic trachybasalts to trachytes (*9, 10, 12–14*). Xenoliths and xenocrysts were recently discovered in these volcanic rocks at eight localities (*12, 14, 15*). We examined inclusions from the north-central part of the Qiangtang terrane (*16*) in an area typified by north-south Pliocene-Quaternary grabens (*17*). We observed basaltic flows overlying relatively fresh, porphyritic, trachyandesite to trachyte flows and rhyolites; broad-beam electron-microprobe analyses show that the trachytic flows are moderately shoshonitic (K_2O/Na_2O = 1.5 to 2.0). Phenocrysts in the

[1]Geological Sciences, University of California, Santa Barbara, CA 93106, USA. [2]Mineralogisch-Petrographisches Institut, University of Bern, Baltzerstrasse 1, CH-3012 Bern, Switzerland. [3]Institut für Geologie, Technische Universität Bergakademie Freiberg, Bernhard-von-Cottastrasse 2, D-9596 Freiberg/Sachsen, Germany. [4]Department of Earth and Space Sciences, 3806 Geology Building, Los Angeles, CA 90095–1567, USA. [5]Geological and Environmental Sciences, Stanford University, Stanford, CA 94305–2115, USA. [6]GeoForschungsZentrum Potsdam, Telegrafenberg A17, 14473 Potsdam, Germany. [7]Institute of Geomechanics, Chinese Academy of Geological Sciences, 11 Minzu Xueyuan Nanlu, Beijing, China, 100081.

shoshonites include plagioclase (An_{28-42}), sanidine (Or_{56-59}), partly resorbed quartz, pargasite, apatite, and abundant partly resorbed biotite. The groundmass is dominated by microcrystalline sanidine, phlogopite, ilmenite, titaniferous magnetite, apatite, and glass (*18*). The more evolved flows locally contain millimeter- to centimeter-sized xenoliths and xenocrysts.

The xenoliths comprise mafic rocks and siliciclastic metasedimentary rocks (*19*). The mafic rocks include biotite-bearing clinopyroxenite and amphibolite in addition to clinopyroxene-orthopyroxene-plagioclase granulites. The metasedimentary samples are dominated by garnet + orthopyroxene + plagioclase + potassium feldspar + quartz ± biotite ± sillimanite ± hercynite ± monazite ± zircon; the most aluminous sample contains cordierite + sillimanite + orthopyroxene + quartz. These mineralogies and mineral compositions clearly demonstrate that the metasedimentary protoliths were pelites and graywackes (*20*). The xenocrysts are mainly sanidine, garnet, biotite, plagioclase, orthopyroxene, and quartz—similar to the phenocryst assemblage in the volcanic rocks except for the addition of garnet.

The mineral textures and compositions provide unambiguous evidence for multistage recrystallization of the xenoliths. The primary recrystallization is characterized by the coexistence of almandine garnet + orthopyroxene + biotite + plagioclase + potassium feldspar ± quartz ± sillimanite ± osumilite in metasedimentary rocks and orthopyroxene + clinopyroxene + plagioclase ± biotite in mafic rocks (*21*). The mafic rocks are unfoliated to weakly foliated and preserve cumulus textures, whereas the metasedimentary rocks exhibit compositional layering, a weak foliation, and granoblastic, equigranular textures typical of granulite-facies rocks.

Many of the xenoliths reveal that higher temperatures succeeded formation of the primary mineral assemblage. This secondary overprinting is defined texturally by the breakdown of phlogopite to orthopyroxene + spinel (*22*) symplectites that are an order of magnitude finer grained (50 to 150 μm) and compositionally different from those in the primary assemblage. The habits and shapes of these reaction products are typical of granulite-facies symplectites developed at H_2O-undersaturated conditions (*23*).

Later, when the xenoliths were entrained in the magma that carried them to the surface, silicate liquid intruded into fractures in the xenoliths, forming pockets of quenched melt and a variety of textural and chemical changes, including dehydration melting of biotite to micrometer-scale orthopyroxene + spinel, growth of clinopyroxene + potassium feldspar by reaction of melt with plagioclase and quartz, growth of new orthopyroxene rims from the melt, formation of monazite rims on spinel, reaction of garnet with the melt to form andesine + biotite + magnetite, formation of coronas tens of micrometers thick of submicrometer-scale plagioclase + spinel + orthopyroxene symplectites along garnet-plagioclase grain boundaries, in situ melting of plagioclase, and dissolution of feldspars and quartz. Xenocrysts within the host volcanic rocks display similar features, including growth of secondary rims on orthopyroxene and plagioclase and resorption of phlogopite and quartz.

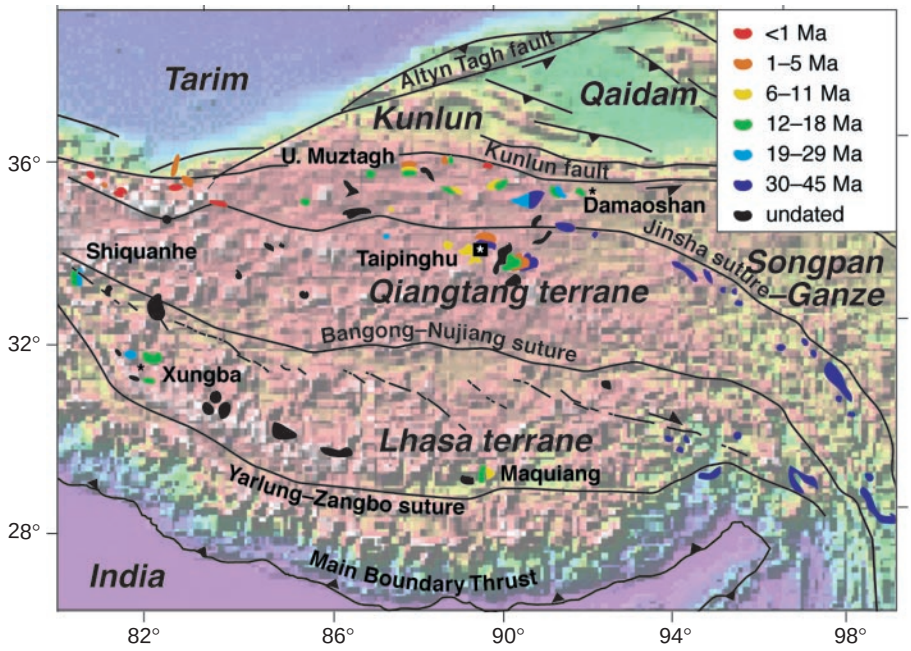

Fig. 1. Volcanic rocks and xenolith localities on the Tibetan plateau (*3, 9, 10, 12–14*). Xenoliths: asterisk, this study; boxed asterisk (*12, 14*). (Inset) Ages of volcanic rocks dated by K/Ar and Ar/Ar methods; fields with ages in multiple ranges are shown schematically.

The mineral compositions and zoning in the Qiangtang xenoliths are compatible with a scenario in which a regional thermal gradient was perturbed more than once by magmatic heat. Recrystallization pressures and temperatures were assessed mostly by partitioning of Al, Fe, and Mg between orthopyroxene and garnet (Fig. 2) (*19*, *24*). Mineral cores in the metasedimentary xenoliths show Fe-Mg apparent temperatures (T_{Mg}) that are colder than Al apparent temperatures (T_{Al}), implying cooling to T_{Mg} from an initial heating to T_{Al} (Fig. 2). Core-to-rim increases in Mg/Fe in garnet and decreases in Mg/Fe in orthopyroxene indicate subsequent heating to 950° to 1300°C (*25*), with $T_{Mg} = T_{Al}$. The preservation of heating-induced zoning at these temperatures requires that the heating lasted <1 My (*26*). The coincidence of rim T_{Mg} and T_{Al} requires rapid cooling of the sort expected during volcanic eruption. Orthopyroxene-clinopyroxene pairs in the mafic xenoliths have homogeneous cores showing T_{Mg} of 850° to 1015°C, and zoned rims, where two pyroxenes are adjacent, showing heating of 35° to 150°C above the core T_{Mg}. Pressures calculated for the metasedimentary xenoliths range from 0.8 to 1.3 GPa, implying extraction depths of about 30 to 50 km.

Two separate sanidine xenocrysts dated by the $^{40}Ar/^{39}Ar$ method yielded ages of 2.5 ± 0.2 Ma and 3.2 ± 0.1 Ma (*27*). These are unambiguously eruption ages of the volcanic rocks because sanidines do not quantitatively retain Ar at the high temperatures demonstrated for these xenoliths. We determined $^{208}Pb/^{232}Th$ ages from 200-μm-diameter monazite inclusions in a 1-cm garnet (12G15A) with an ion microprobe (*19*, *28*). The garnet contains cracks that intersect all the monazite inclusions, and the cracks exhibit alteration associated with silicate melt intrusion. The monazites exhibit U zoning and sector and oscillatory zoning visible with back-scattered electron imaging. Two monazites with dentate grain boundaries show a range in $^{208}Pb/^{232}Th$ spot ages from about 14.2 to 4.2 Ma. A subhedral, equant grain, part of a polymineralic inclusion intruded by melt, gave five spot ages of about 3.4 Ma, and spot ages from a second, texturally similar, monazite grain range from 16.2 to 4.5 Ma. We interpret these textures and ages to indicate Pb loss at about 3.4 Ma. Calculations show that 200-μm monazite grains will lose all their Pb in much less than 1 My if subjected to temperatures >900°C (*29*), confirming that the highest temperatures experienced by the Qiangtang xenoliths were transient.

We interpret the history of the Qiangtang xenolith suite to be (i) deposition of the metasedimentary rocks on Earth's surface; (ii) burial, muscovite-dehydration melting, and extraction of leucogranitic liquids (*30*); (iii)

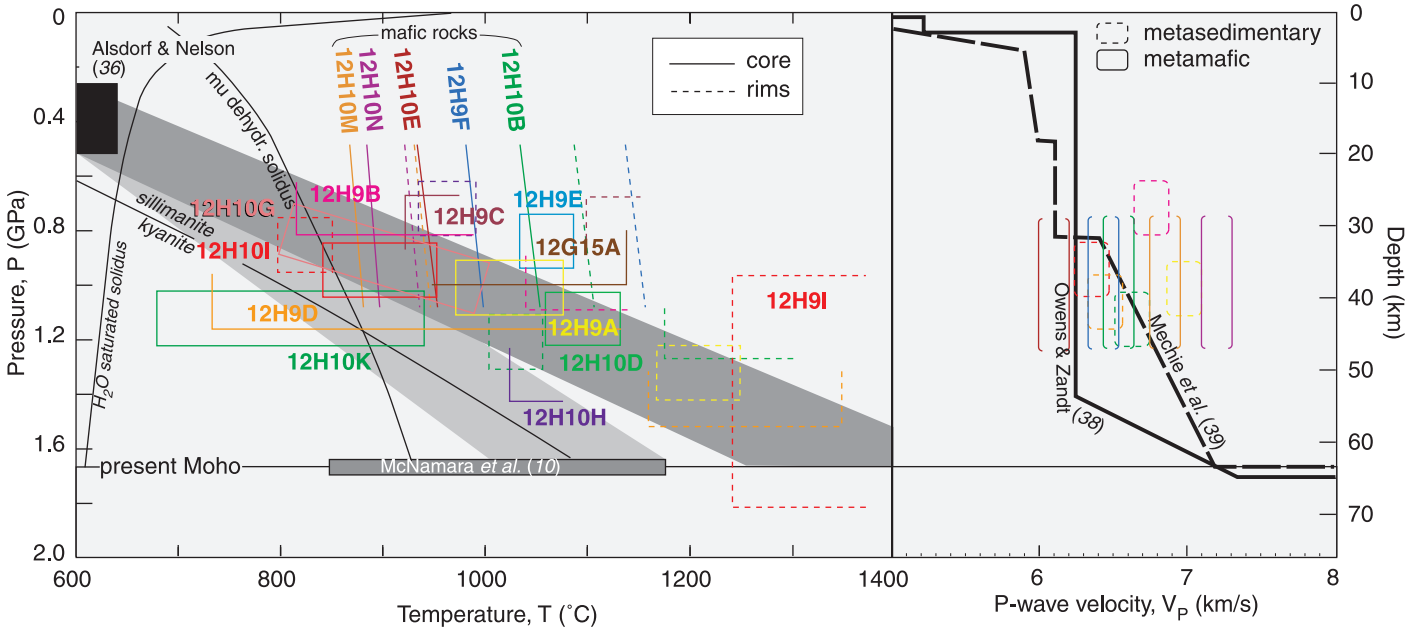

Fig. 2. Tibetan xenolith thermobarometry (*39*) and calculated *P*-wave velocities (*34*). Pale and medium gray bands show inferred "normal" and magmatically elevated thermal gradients, respectively.

attainment of the characteristic granulite-facies metamorphism at 800° to 900°C, biotite-dehydration melting and fluorination of remaining biotite; (iv) additional reaction, including the breakdown of F-biotite and dissolution of feldspar and quartz at 1300°C caused by injection of magma into the lower crust; followed shortly by (v) decompression and quenching during eruption about 3 Ma. That these conclusions pertain to a broad area of the plateau and may reach as far back in time as 15 Ma is suggested by almandine + spinel + sillimanite xenoliths in 15-Ma volcanic rocks (*12*) about 300 km northeast of our locality (Fig. 1).

The xenolith temperatures indicate that a thermal gradient of 17°C per kilometer has prevailed since at least 3 Ma. Seismic data suggest that the present temperature of the uppermost mantle beneath Qiangtang is 840° to 1170°C (*31*). Satellite magnetic data suggest that temperatures > 550°C prevail across the Tibetan Plateau at depths of 15 ± 5 km (Fig. 2), and this places the H_2O-saturated granite solidus at a depth of 17 ± 5 km across the plateau, such that melt may be present below this depth across the entire plateau (*32*). The slower-than-normal seismic wave speeds and somewhat high Poisson's ratio of the crust imply the presence of partial melt (*33*). The xenolith suite shows, however, that although the Qiangtang lower crust is at temperatures above the solidus of H_2O-saturated continental crustal rocks—indeed, above the dehydration-melting solidus of mica (Fig. 2)—and has been since 3 Ma, the nearly anhydrous character of the xenoliths (the OH in biotite having been replaced by F, for example) means that the crust need not be molten in spite of the extreme temperatures. Moreover, the seismic wave speeds and Poisson's ratios we calculate for the xenoliths, considering only their crystalline phases and excluding melt (Fig. 2) (*19*), straddle those from seismological models of Qiangtang terrane (*33*–*35*).

Turner *et al.* (*13*) interpreted Tibetan potassic lavas to have been generated by partial melting of enriched mantle, in part because of high K_2O and light rare-earth-element concentrations, radiogenic Sr and Pb isotopic ratios, and relatively unradiogenic Nd. However, if the lower crust of Tibet is partly metasedimentary, instead of wholly gabbroic, and is hot, mantle-generated melts that traverse the lower crust will have considerably different interaction with the lower crust than is commonly considered. Indications of in situ melting of biotite, feldspar, and quartz in the metasedimentary xenoliths, and of resorption of biotite, feldspar, and quartz in the volcanic rocks hosting the xenoliths, reveal that partial melting of the xenoliths or other metasedimentary rocks contributed some silicate liquid to the mantle-derived magma. The widespread occurrence of fine-grained, undigested xenocrysts suggests that the unusual chemical patterns of some Tibetan lavas may be a mixture of lower Tibetan crustal fragments with a mantle-derived melt. Moreover, Patiño Douce and McCarthy (*36*) showed that dehydration melting of mica—the melting documented in the Qiangtang xenoliths—produces (ultra)potassic melts and garnet-cordierite-orthopyroxene–rich residues. Such rocks would have previously undergone H_2O-saturated melting to yield trondhjemitic liquids and mica-rich residues; this inferred early melting event could have occurred either during introduction to the deep crust if the protolith was low-grade sediments such as the Songpan-Ganze flysch (*37*) or possibly long before if the protolith metasedimentary rocks were already dry granulites. Surface geologic exposures have been used to infer that upper crustal lithologies are widespread beneath central and northern Tibet (*37*); if so, the currently popular model for the Tibetan ultrapotassic-shoshonitic volcanism, melting of enriched lithospheric mantle due to convective thinning of its lower parts, should be reconsidered.

As an alternative to convective thinning of the mantle lithosphere, Deng (*3*) suggested that potassic volcanism on the plateau is linked to intracontinental subduction. This idea received support from Meyer *et al.* (*4*), who proposed that the distribution and age of plateau volcanism is directly linked to successive episodes of upper-middle crustal shortening accommodated by intracontinental subduction of lower crust and mantle, and from Kapp *et al.* (*37*), who proposed that the Songpan-Ganze flysch was thrust beneath Qiangtang in the early Mesozoic, and later catalyzed Cenozoic volcanism. The pattern of volcanism on the plateau (Fig. 1) (*38*) suggests a meld of both models: from 30 to 45 Ma volcanism straddled the Jinsha suture in eastern Tibet, between 29 and 6 Ma volcanic rocks erupted in a small area southwest of the Kunlun fault, and subsequent eruptions have occurred in the same area as well as farther west. If the pattern of volcanism can be used as a guide, the major changes in the evolution of the plateau distal to the Himalayan front occurred at 30 and 5 Ma.

References and Notes

1. E. Argand, *Proc. 13th International Geological Congress* (1924), p. 171; M. Barazangi and J. Ni, *Geology* **10**, 179 (1982).

2. W.-L. Zhao and W. J. Morgan, *Tectonics* **4**, 359 (1983); R. Westaway, *J. Geophys. Res.* **100**, 15173 (1995).
3. W. Deng, *Chinese J. Geochem.* **10**, 140 (1991).
4. B. Meyer *et al.*, *Geophys. J. Int.* **135**, 1 (1998).
5. J. F. Dewey, R. M. Shackleton, C. Chang, Y. Sun, *Philos. Trans. R. Soc. London Ser. A* **327**, 379 (1988).
6. M. A. Edwards and T. M. Harrison, *Geology* **25**, 543 (1997).
7. M. A. Murphy *et al.*, *Geology* **25**, 719 (1997).
8. F. M. Richter, O. M. Lovera, T. M. Harrison, P. Copeland, *Earth Planet. Sci. Lett.* **105**, 266 (1991); C. Mock, N. O. Arnaud, J.-M. Cantagrel, *Earth Planet. Sci. Lett.* **171**, 107 (1999).
9. N. O. Arnaud *et al.*, *Earth Planet. Sci. Lett.* **111**, 351 (1992); S. Turner *et al.*, *Nature* **364**, 50 (1993).
10. S. L. Chung *et al.*, *Nature* **394**, 769 (1998).
11. A. Lenardic and W. M. Kaula, *J. Geophys. Res.* **100**, 15193 (1995). There are other reasons to question the convective thinning model. For example, it does not explain why Miocene-Recent magmatism is localized along the Plateau edges (Fig. 1) or why the warm area of the mantle inferred by (*30*) on the basis of slow *S* wave propagation does not correspond more closely to the region of recent volcanism. Moreover, geomorphological evidence of the sudden uplift predicted by the model has not been observed—at least not in the northeastern part of the plateau (*4*).
12. W. Deng, *Acta Petrol. Mineral.* **15**, 289 (1996).
13. S. Turner *et al.*, *J. Petrol.* **37**, 45 (1996).
14. C. Miller *et al.*, *J. Petrol.* **40**, 1399 (1999).
15. International Deep Profiling of Tibet and the Himalaya (INDEPTH) 1998 and 1999 geologic field parties.
16. The xenoliths were found near 34°24′N, 89°14′E, southeast of Lake Dogai Coring in a volcanic field that apparently corresponds to the Taipinghu field of Deng [*Proc. 30th International Geological Congress* **15**, 3 (1997)] and area VIII of Turner *et al.* (*13*).
17. Graben age is based on scarp morphology and a 3.9 ± 0.4 Ma $^{40}Ar/^{39}Ar$ age we obtained on muscovite vein fill in a fault breccia [S. Bi *et al.*, *Eos* **80**, F1015 (1999)].
18. These volcanic rocks are distinct from those reported by Turner *et al.* (*13*), which typically contain clinopyroxene, only rare biotite, and no amphibole. They are also distinct from the rhyolitic tuffs investigated by L. W. McKenna and J. D. Walker [*J. Geophys. Res.* **95**, 21483 (1990)], which contain cordierite and tourmaline. Electron-probe analyses of ground mass glass show 70 to 75 weight percent (wt%) SiO_2, 9 to 10 wt% Al_2O_3, 0.5 to 2.2 wt% CaO, 1.6 to 3 wt% Na_2O, 4 to 9 wt% K_2O, and <0.5 wt% FeO + MgO. Biotite phenocrysts contain 3 to 4 wt% TiO_2 and 5 to 7 wt% F.
19. Supplementary material is available at www.sciencemag.org/feature/data/1046489.shl.
20. All the xenoliths were derived from the crust. Olivine-rich, eclogitic, carbonate, and quartzite xenoliths were not found. Some samples can be described as tonalites and have mineralogies that at first glance suggest an igneous origin, but the presence of low-Ca, high-Mn garnet and hercynitic spinel, and the absence of clinopyroxene, suggest that these are metasedimentary and may be residua after partial melting.
21. Metasedimentary rocks contain $Alm_{48-76}Prp_{12-58}Grs_{03-10}Sps_{01-09}$ garnet, $Fs_{39-76}En_{17-67}Wo_{01-03}$ orthopyroxene, Mg_{72-89} biotite, $An_{13-48}Or_{03-25}Ab_{47-68}$ plagioclase, $An_{01-04}Or_{45-65}Ab_{31-52}$ anorthoclase-sanidine, and Mg_{73} cordierite. Mafic rocks contain $An_{34-91}Or_{01-08}Ab_{08-57}$ plagioclase, $Fs_{23-43}En_{63-72}Wo_{01-03}$ orthopyroxene, $Fs_{01-30}En_{20-55}Wo_{41-79}$ clinopyroxene, and Mg_{72-75} biotite (Ab, albite; Alm, almandine; An, anorthite; En, enstatite; Fs, ferrosilite; Grs, grossular; Or, orthoclase; Prp, pyrope; Sps, spessartine; Wo, wollastonite).
22. Hercynite is $(Mg_{0.2-0.4}Fe_{0.8-0.6}Fe_{0.1-0.5}Al_{0.9-0.5})O_4$ and magnetite-ulvospinel is $(Mg_{0.1}Fe_{0.9})(Fe_{1.0-1.5}Al_{0.5-1.0})O_4$
23. S. L. Harley, in *What Drives Metamorphism and Metamorphic Reactions?*, P. J. Treloar and P. J. O'Brien, Eds. (Geological Society, London, 1999), vol. 138, pp. 81–107.
24. We determined equilibration pressures and temperatures chiefly by Fe-Mg exchange between clinopyroxene and orthopyroxene [G. P. Brey and T. Koehler, *J. Petrol.* **31**, 1353 (1990)]; Fe-Mg exchange between garnet and orthopyroxene; Al solubility in orthopyroxene in the presence of garnet; Al solubility in orthopyroxene in the presence of garnet, plagioclase, and quartz (GOPS); and CaAl net transfer between garnet and plagioclase in the presence of sillimanite and quartz (GASP) [A. M. Koziol and R. C. Newton, *Contrib. Mineral. Petrol.* **103**, 423 (1989)]. The GOPS and GASP calculations were done with the program GTB 2.1 [M. Kohn and F. Spear, www.rpi.edu/dept/geo/spear/GTB_Prog/GTB.html (1998)]. The positions of all these reactions were also calculated with Thermocalc 2.7 and its 1998 database [T. J. B. Holland and R. Powell, *J. Metamorph. Geol.* **16**, 309 (1998)]. We calculated garnet-orthopyroxene Fe-Mg exchange temperatures with four different calibrations [S. L. Harley, *Contrib. Mineral. Petrol.* **86**, 359 (1984); D. A. Carswell and S. L. Harley, in *Eclogite Facies Rocks*, D. A. Carswell, Ed. (Blackie, Glasgow, 1990), pp. 83–110; H. Y. Lee and J. Ganguly, *J. Petrol.* **29**, 93 (1988); J. O. Eckert Jr., R. C. Newton, O. J. Kleppa, *Am. Mineral.* **76**, 148 (1991)], which yielded a 100° to 200°C temperature range; we chose the mean of the hottest and coldest temperatures as the representative value. We prefer the newest Al thermometer [L. Y. Aranovich and R. G. Berman, *Am. Mineral.* **82**, 345 (1997)] to that of Harley and Green [S. L. Harley and D. H. Green, *Nature* **300**, 697 (1982)]. GOPS pressures calculated by the Moecher *et al.* [D. P. Moecher, E. J. Essene, L. M. Anovitz, *Contrib. Mineral. Petrol.* **100**, 92 (1988)] and Eckert and Bohlen [J. O. Eckert Jr. and S. R. Bohlen, *Geol. Soc. Am. Abstr. Prog.* **30** (1998)] calibrations differ by 0.2 to 0.4 GPa; to be conservative, we have chosen the latter, which yields lower pressures and hence lower temperatures for most samples.
25. These high temperatures are reinforced by the observation that the nominally hydrous minerals in the xenoliths are fluorinated. The biotite crystals, whose breakdown marks the secondary overprinting, contain 4 to 9 wt% TiO_2 and 4 to 7 wt% F, both of which increase thermal stability: dehydration melting of F-poor biotites occurs at 900° to 1000°C, whereas fluorinated biotite can be stable to 1300°C [D. F. Dooley and A. F. Patiño Douce, *Am. Mineral.* **81**, 202 (1996)]. Similarly, fluorinated hornblende (2 wt% F), present in sample 12H10H, is stable to temperatures as high as about 1200°C [J. R. Holloway and C. E. Ford, *Earth Planet. Sci. Lett.* **25**, 44 (1975)].
26. J. Ganguly and M. Tirone, *Earth Planet. Sci. Lett.* **170**, 131 (1999).
27. The sanidines were loose macrocrysts and their difference in ages suggests that they were derived from two separate flows. The grains were crushed to about 200 μm and then step heated and individually fused with a laser at Stanford University by procedures outlined in Hacker *et al.* [B. R. Hacker, J. L. Mosenfelder, E. Gnos, *Tectonics* **15**, 1230 (1996)]. We also dated sanidine and hornblende from cobbles of hypabyssal biotite-hornblende syenodiorite to quartz diorite in a river draining a multisummit volcanic edifice at 34°22′N, 89°28′E that appeared from Landsat multispectral scanner images to possibly be the source of the xenolith-bearing flows. These samples gave older ages of 34 to 36 Ma, although they show the same chemical characteristics as the volcanic rocks (*11, 12, 31*): 54 to 68 wt% SiO_2, 4.5 wt% K_2O, 1100 to 1800 parts per million (ppm) of Ba, 400 to 1200 ppm of Sr, and 130 to 280 ppm of Rb (determined by x-ray fluorescence at Bern University).
28. A sectioned and polished garnet characterized by scanning electron microscopy and electron-probe microanalysis was mounted in epoxy alongside previously polished grains of 554 standard monazite (45 ± 1 Ma). The composite mount was ultrasonically cleaned in ethanol, oven dried at 80°C, and coated with about 50 Å of Au. A mass resolution of 4500 was used to separate molecular interferences for ^{204}Pb and ^{208}Pb, and apertures were set to block secondary ions emitted from the margins of the 15-μm-diameter beam formed by the 6-nA O primary beam [(T. M. Harrison *et al.*, *Earth Planet. Sci. Lett.* **146**, E1 (1997)]. When combined with O_2 flooding (3×10^{-5} torr) of the sample surface, these instrument settings were sufficient to yield $^{208}Pb^+$ intensities high enough that $^{208}Pb/^{232}Th$ age determinations of these youthful monazites performed over 15 min were limited primarily by the reproducibility of the ThO_2^+/Th^+ versus Pb^+/Th^+ calibration curve determined from monazite standard 554 instead of by counting statistics. A relatively high radiogenic ^{208}Pb yield of 90% means that the calculated ages are insensitive to our assumed common $^{208}Pb/^{204}Pb$ ratio of 37.9. Our ability to reproduce the age of monazite standard 554 (2.2%, 2σ) was similar to that obtained for apparently homogeneous regions of the unknown monazite (1 to 2%). A complete data tabulation is available at http://oro.ess.ucla.edu.
29. H. A. Smith and B. J. Giletti, *Geochim. Cosmochim. Acta* **61**, 1047 (1997).
30. There is no direct textural evidence that dehydration melting of muscovite occurred in these rocks, but the absence of muscovite in such a bulk composition and the certainty that the rocks passed through conditions conducive to dehydration melting of muscovite renders it almost certain. Whether such an event occurred long before burial beneath the Qiangtang or occurred during burial to lower crustal depths beneath Qiangtang is unknown.
31. D. E. McNamara, W. R. Walter, T. J. Owens, C. J. Ammon, *J. Geophys. Res.* **102**, 493 (1997).
32. D. Alsdorf and D. Nelson, *Geology* **27**, 943 (1999).
33. T. J. Owens and G. Zandt, *Nature* **387**, 37 (1997); A. J. Rodgers and S. Y. Schwartz, *J. Geophys. Res.* **103**, 7137 (1998).
34. Seismological studies (*33*) have derived average Qiangtang crustal properties of V_P = 6.1 to 6.3 km/s, V_S = 3.3 to 3.4 km/s, and Poisson's ratio = 0.28 to 0.30. A recent, detailed crustal model based on wide-angle data (*35*) shows the same average crustal P-wave velocity (6.2 km/s) and average velocities of 6.5 to 6.6 km/s over the depth range sampled by our xenoliths (30 to 50 km). Our calculations of xenolith physical properties, based on Sobolev and Babeyko [S. V. Sobolev and A. Yu. Babeyko, *Surv. Geophys.* **15**, 515 (1994)] indicate V_P = 6.1 to 7.2 km/s, with an average of 6.6 km/s (*19*), in agreement with the seismic model (*35*). Our calculated Poisson's ratios range from 0.258 to 0.272 with an average of 0.266; such high Poisson's ratios derive from the abundance of feldspar, garnet, and beta quartz, which all have relatively high V_P/V_S. Note that this calculated Poisson's ratio is a minimum, as our calculations do not include anelasticity, which can increase the Poisson's ratio of long-period teleseismic waves by 0.01 to 0.02 in hot but unmelted rocks [S. V. Sobolev *et al.*, *Earth Planet. Sci. Lett.* **139**, 147 (1996)].
35. J. Mechie *et al.*, *Eos* **80**, F951 (1999).
36. A. E. Patiño Douce and T. C. McCarthy, in *When Continents Collide: Geodynamics and Geochemistry of Ultrahigh-Pressure Rocks*, B. R. Hacker and J. G. Liou, Eds. (Kluwer Academic, Dordrecht, Netherlands, 1998), p. 27.
37. P. Kapp *et al.*, *Geology* **28**, 19 (2000).
38. If the unusual rocks in the south and west are not considered. Whereas most Tibetan volcanic rocks are shoshonitic to ultrapotassic trachybasalts to trachytes, there are unusual peraluminous rhyolites at Ulugh Muztagh that are inferred to be crustal melts [W. McKenna and J. D. Walker, *J. Geophys. Res.* **95**, 21483 (1990)], lavas at Shiquanhe and Xungba with distinctly evolved Nd and Sr isotopic ratios that suggest crustal contamination (*12, 13*), and high-K calc-alkaline volcanics at Maquiang that have distinctly primitive Nd and Sr isotopic ratios [C. Coulon, H. Maluski, C. Bollinger, S. Wang, *Earth Planet. Sci. Lett.* **79**, 281 (1986)].
39. Temperature ranges encompass only intrasample variation and do not include analytical or calibration accuracy. Pressures are shown with a nominal 100-MPa uncertainty. Black box shows conditions inferred by Alsdorf and Nelson (*32*) on the basis of satellite magnetic data. Solidi are from Patiño Douce and McCarthy (*36*) and Johannes and Holtz [W. Johannes and F. Holtz, *Petrogenesis and Experimental Petrology of Granitic Rocks* (Springer-Verlag, Heidelberg, 1996)].

40. Funded by NSF grant EAR-9728643 and Deutsche Forschungsgemeinschaft grant Ra442/12-1. Thanks to our INDEPTH III colleagues P. Blisniuk, M. Edwards, W. Kidd, O. Kuchel, L. Jixiang, B. Siwen, M. Staiger, and L. Youshe, who helped collect xenoliths under difficult conditions. Reviewed by G. Ernst, J. Liou, D. Nelson, R. Rudnick, and A. Yin.

22 October 1999; accepted 18 January 2000